



# Frequency and peak discontinuities in self-pulsations of a CO<sub>2</sub> laser with feedback

Leandro Junges<sup>a,b</sup>, Jason A.C. Gallas<sup>a,b,c,\*</sup>

<sup>a</sup> Institute for Multiscale Simulation, Friedrich-Alexander Universität, Nögelsbachstraße 49b, 91052 Erlangen, Germany

<sup>b</sup> Instituto de Física, Universidade Federal do Rio Grande do Sul, 91501-970 Porto Alegre, Brazil

<sup>c</sup> Departamento de Física, Universidade Federal da Paraíba, 58051-970 João Pessoa, Brazil

## ARTICLE INFO

### Article history:

Received 24 May 2012

Received in revised form

12 June 2012

Accepted 14 June 2012

Available online 29 June 2012

### Keywords:

Self-pulsing

Laser stability diagrams

Optical instabilities

CO<sub>2</sub> lasers with feedback

Peak-adding cascades

## ABSTRACT

We show that self-pulsations observed in a CO<sub>2</sub> laser with feedback display two types of recurrent period discontinuities when control parameters are changed. Periodic self-pulsations emerge organized in wide adjacent phases in which oscillations differ by a constant number of peaks in their period. The number of peaks increases through characteristic *pulse deformations* of the signal that we describe in detail. The passage across the boundaries delimiting adjacent phases is abrupt and not mediated by windows of chaos. In addition, we provide an explicit criterion for locating the discontinuity boundaries between adjacent phases.

© 2012 Elsevier B.V. All rights reserved.

## 1. Introduction

A standard way to stabilize and control the output frequency, wavelength and power of a laser is by using feedback loops, either optical, electronic, or electrooptical [1]. The efficient design of suitable feedback loops requires an understanding of the impact of parameter changes. In fact, lack of such information makes it quite unclear how to optimize system operation in order to further develop quantum electronics and laser applications. While the possible dynamical behaviors of lasers were classified in great detail for many situations of interest [2,3], parameters considered were essentially restricted to a few specific *ad hoc* values or intervals. Most laser systems still lack an encompassing and systematic analysis of their control parameters classifying the nature and relative abundance of their stable pulsations.

The aim of this paper is to report stability diagrams characterizing the nature and the global distribution of self-pulsations in a class-B laser with optical feedback when more than one parameter is varied simultaneously. The working system considered here is a familiar model of a CO<sub>2</sub> laser with a feedback loop [4–7]. The control parameter space of this system was considered before by Yang et al. [6] with a much higher level of detail than usual for laser systems. These authors performed the standard linear stability analysis and identified the boundaries between stable

and unstable fixed-point (i.e. non-oscillatory) solutions of the laser. However, they also computed numerically the period and the number of peaks of the laser intensity as a function of two parameters,  $r$  (feedback gain) and  $B$  (bias voltage), as defined below in Eqs. (1)–(3). They observed that an increase in the feedback gain,  $r$ , results in an increase in the number of peaks of the laser intensity and found that an increase of the bias voltage,  $B$ , induces an increase in the period of the signal. They observed a divergence of the self-pulsing period  $T$  when increasing  $B$  after fixing  $r$  at a particular value, viz.  $r=0.21593$ .

The aim of this paper is to complement and extend the pioneering work of Yang et al. [6]. The reason for this is the recent upsurge of interest in studying the structure of parameter space of laser systems due to both, the availability of more powerful computers, and the development of automated techniques to record experimental data. As one specific example, we mention very recent interesting work of Toomey et al. [8] reporting automated protocols to characterize experimental time series data for optically injected VCSELs in terms of stability. Here, for the CO<sub>2</sub> laser we show that, first, in addition to the period divergence observed by Yang et al. while tuning a single parameter ( $B$ ), the laser displays a rather distinct type of discontinuities when  $B$  and  $r$  are tuned simultaneously. Furthermore, we find the laser self-pulsing to display a plethora of intricacies and discontinuities not only in the period (frequency) as observed before, but also in the intensity and in the number of peaks of periodic pulses. High-resolution stability diagrams in the  $r \times B$  control plane reveal that sharp discontinuities in the number of peaks form the boundaries of wide regions of stability, or phases.

\* Corresponding author at: Instituto de Física, Universidade Federal do Rio Grande do Sul, 91501 970 Porto Alegre, Brazil. Tel.: +55 51 3308 6522; fax: +55 51 3308 7286.

E-mail address: [jgallas@if.ufrgs.br](mailto:jgallas@if.ufrgs.br) (J.A.C. Gallas).

The number of peaks increases abruptly at the phase boundaries as control parameters are changed (see Fig. 1). The location of such boundaries requires tuning more than one parameter. Second, while the laser contains a relatively narrow chaotic phase, we show such phase to be about an order of magnitude larger than previously observed by Yang et al. [6]. Further, instead of a single islands of chaos, we find what appears to be an infinite sequence of relatively similarly looking sequence of islands. We find such chaotic phases to be riddled with large islands characterized by periodic self-pulsations as described below.

While studying the pattern evolution of the laser self-pulsations we observed that their number of peaks increases systematically in a very specific way, through certain characteristic *pulse deformations* which we describe below in detail. Thus, bifurcation diagrams of the laser intensity are shown to contain a remarkable feature: the intensity undergoes peak-adding bifurcations mediated by pulse deformations, not by windows of chaos, as it is usual. We establish an explicit criterion, Eq. (6), allowing one to locate pulse discontinuities, i.e. to determine the birth of new peaks in self-pulsations. The present work also serves an additional purpose, namely to provide reference stability diagrams against which to compare phase diagrams obtained for much more complicated models of the laser, including situations involving the presence of a *delayed*

feedback, a classical problem in the field [9–13] that has great technological interest for practical applications like, e.g. secure communications [14–19]. In a separate work we report phase diagrams for the same model studied here but taking also into account the effect of a delayed feedback [20].

## 2. The CO<sub>2</sub> laser with feedback

The model of the CO<sub>2</sub> laser with feedback of interest to us is described by three autonomous coupled differential equations involving three variables and seven parameters. Calling  $x(t)$  the laser intensity normalized to the saturation value,  $y(t)$  the population inversion normalized to the threshold value, and  $z(t)$  the feedback voltage normalized to  $1/\pi$  times the voltage of the electro-optic modulator, the governing equations can be written as [4–7]

$$\dot{x} = kx(y - 1 - \alpha \sin^2 z), \quad (1)$$

$$\dot{y} = \gamma(A - y - xy), \quad (2)$$

$$\dot{z} = \beta(B - rx - z), \quad (3)$$

here  $k$  stands for the unmodulated cavity loss,  $\gamma$  is the population decay rate,  $\beta$  is the damping rate of the feedback loop,  $r$  is the

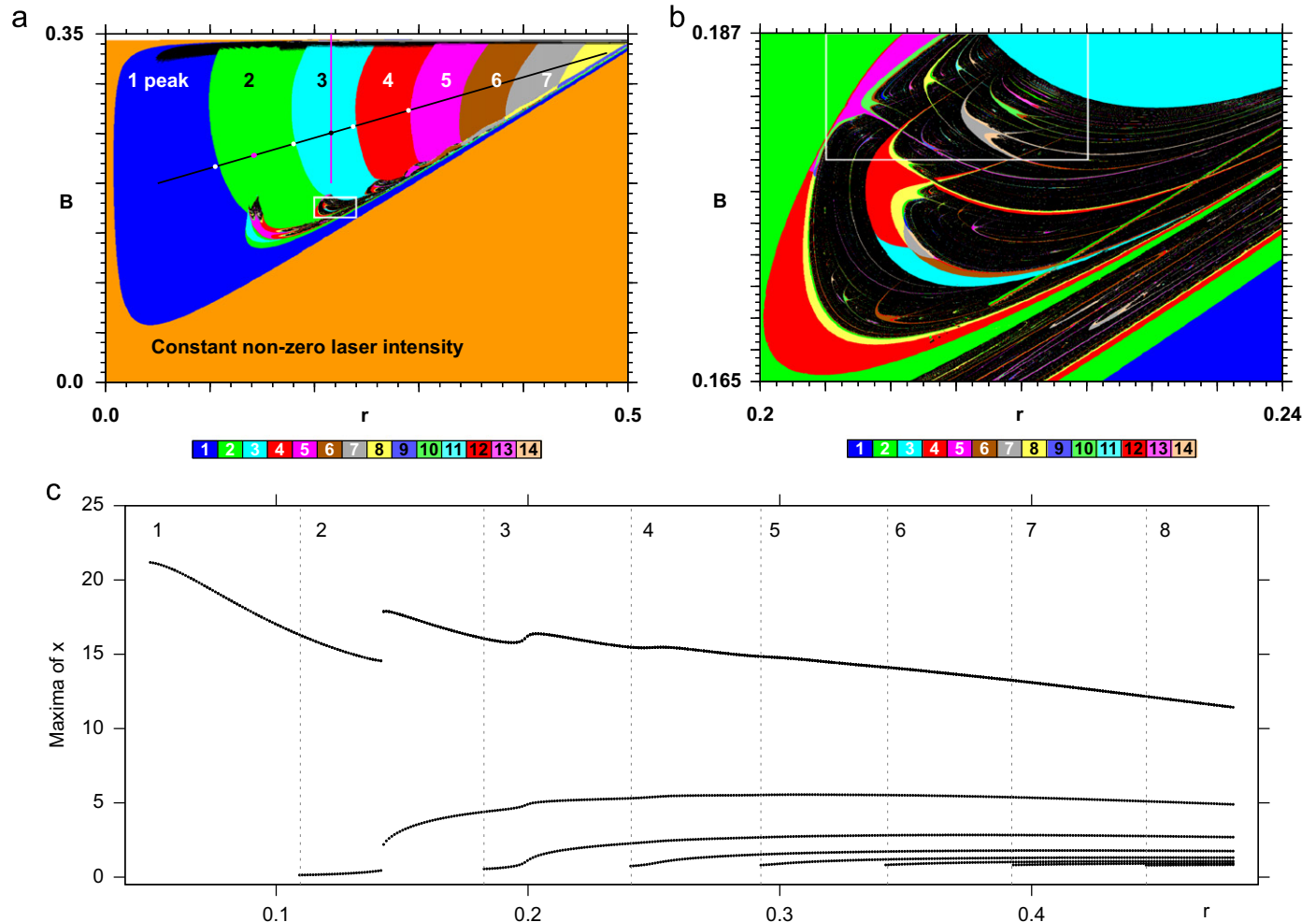


**Fig. 1.** (a) Stability diagram classifying self-pulsating oscillations according to the number of peaks of the laser intensity,  $x(t)$  in Eq. (1), as indicated by the numbers. Black denotes regions of chaotic oscillations. Black is also used in the horizontal stripe seen in the upper part of the figure to represent periods  $T > 400$ , i.e. the divergence of the period. The narrow white stripe on the top marks zero intensity solutions (laser off). The points and pair of lines are discussed in subsequent figures (see text). (b) Magnification of the white box in (a) showing the same mosaic pattern reported recently for delay-differential equations [22] and standard accumulations of shrimps (see text). The box is shown magnified in Fig. 5. (c) Bifurcation diagram showing the peak-adding cascade in  $x(t)$  along the black line in (a), Eq. (4), as indicated by the numbers. The laser intensity undergoes peak-adding cascades mediated by pulse deformations, not by windows of chaos, as usual. See text.  $B$  and  $r$  are in the same units of Refs. [4–6].

feedback gain,  $B$  is the bias voltage applied to an electro-optic modulator,  $A$  is a normalized pump parameter, and  $\alpha$  is the amplitude of the modulation [5]. Following Yang et al. [6], we focus on the  $r \times B$  control plane and fix  $A=1.66$ ,  $\alpha=5.8$ ,  $k=9.6 \times 10^{-6} \text{ s}^{-1}$ ,  $\gamma=0.03 \times 10^{-6} \text{ s}^{-1}$ ,  $\beta=0.5 \times 10^{-6} \text{ s}^{-1}$ . As usual,  $B$  is normalized to  $1/\pi$  times the half wavelength voltage of the modulator [4–6].

The laser model of Eqs. (1)–(3) has already been extensively studied since first introduced [4,5], and forms the basis for more complicated situations, when delayed feedback is also included [13–20]. This is the reason of our interest in classifying its dynamical properties over extended regions of the control parameters. Detailed knowledge of such predictions for this paradigmatic model is of course necessary to assess the need for better models and the impact of changes associated with them.

### 3. Peak-adding not mediated by chaos

Fig. 1(a) and (b) shows stability diagrams obtained numerically by solving Eqs. (1)–(3) using a fixed-step  $h=0.002$  fourth-order Runge–Kutta algorithm on a grid of  $1200 \times 1200 = 1.44 \times 10^6$  equally spaced points  $(r, B)$ . We started numerical integrations from the initial conditions  $(x(0), y(0), z(0)) = (1.0, 1.0, 1.0)$ . However, taking them randomly, uniformly distributed in the interval  $[0, 1]$ , produces virtually indistinguishably similar diagrams. The integration is numerically a quite demanding task, performed on a cluster of 700 high-performance processors. For each solution we counted the number of peaks of  $x(t)$  and recorded whether pulses repeated or not.

Periodic pulsations were represented using 14 colors, as indicated by the color-bar in the figures (described in detail elsewhere [21]), to reflect the number of peaks within their period. Pulses having more than 14 peaks were plotted “recycling colors mod 14”, i.e. taking as the color index the remainder of the integer division of the number of peaks by 14. Multiples of 14 were given the index 14. In this way all periodic pulses could be accommodated with the 14 colors available. Lack of numerically detectable periodicity was interpreted as “chaos” and plotted in black. Fixed points (i.e. non-oscillatory laser intensity) were plotted using two additional colors: the color of the large domain marked “constant non-zero laser intensity” in Fig. 1(a), and white, to represent  $x=0$  no-lasing solutions. The no-lasing solutions appear as a very narrow white horizontal stripe at the top of Fig. 1(a).

Fig. 1(a) and (b) shows how self-pulsations are distributed and organized in control parameter space. Fig. 1(a) displays a sequence of adjacent regions containing numbers denoting the number of peaks of the laser intensity. This organization agrees well with Fig. 3 of Yang et al. [6] but considerably extends it, indicating that chaos is more abundant than originally found and that it recurs regularly in control parameter space. In addition, Fig. 1(b) illustrates details of the inner structure of one of the chaotic windows, the one inside the white box in Fig. 1(a), showing that chaotic laser phases have a quite complex inner organization, riddled by the familiar *shrimp* sequences [23–27], namely by sequences of islands where we find periodic self-pulsations which unfold in a complex and specific way, via the pulse deformations described in the next section. As may be seen from Fig. 1(b), the control parameter space has specific boundaries where the *shrimp* sequences accumulate [28]. The peculiar adjacent arrangement of isospike regions in Fig. 1(a) shows a subtle behavior, namely, a peak-adding cascade where the number of peaks grows arithmetically, not geometrically as for the more frequently observed period-doubling cascade. More importantly, the several isospike windows are not separated by windows of chaos as it is more common for adding cascades (see Fig. 5 below) but, instead, here the number of peaks increases

abruptly from window to window, without any trace of chaos between them.

Fig. 1(a) contains a black line defined by the equation

$$B = 0.184756 + 0.304878r, \quad 0.05 < r < 0.48. \quad (4)$$

Along this line we computed the bifurcation diagram shown in Fig. 1(c), which illustrates in more detail how the number of peaks vary when two parameters are tuned simultaneously. As it is easy to realize from Fig. 1(a), the bifurcation diagram presented is representative of the diagrams obtained along most lines of constant  $B$ , which display nothing else than a more restricted unfolding of the bifurcation cascade.

### 4. Pulse deformations and isolated branches

In the previous section we saw that the bifurcation diagram of Fig. 1(c) contains several *isolated branches*, namely single branches that start quite abruptly for specific values of  $r$  and result in an atypical peak-adding cascade, not mediated by chaos. We now show that such isolated branches arise from *pulse deformations* when parameters evolve. We also provide an explicit criterion, Eq. (6), allowing one to determine the emergence of new peaks in self-pulsations.

Fig. 2(a)–(d) displays examples of self-pulsations for  $r=0.105$ ,  $0.180$ ,  $0.237$ ,  $0.290$  and  $B$  as defined by Eq. (4). These four points are indicated by white dots on the black line in Fig. 1(a). They are located immediately before the boundaries marking a change in the number of peaks of the laser intensity. Fig. 2(a)–(d) also contains a vertical arrow to indicate the location of a “precursor” of a peak, i.e. the position where a new peak will arise when  $r$  is increased slightly. The explanation of the successive peak creation can be given referring to Fig. 2(e)–(h), on the right column.

Fig. 2(e)–(h) shows two curves in the  $y \times z$  plane. The first one, represented as a light parabolic arc, marks the solution of  $f(y, z) = 0$ , where

$$f(y, z) = y - 1 - \alpha \sin^2 z. \quad (5)$$

This function is one of the two factors which appear in  $dx/dt$  (see Eq. (1)). The other curve records the locus  $(y, z)$  obtained by integration of Eqs. (1)–(3).

The characteristic signature of the birth of a new isolated branch in the bifurcation diagram is the occurrence of *intersection points* between these two curves as parameters are tuned. The arrows in Fig. 2(e)–(h) show where new intersections will occur when  $r$  is increased. Such intersections are responsible for the several isolated branches seen at the bottom of the bifurcation diagram in Fig. 1(c). Thus, the condition for the genesis of new isolated branches in the bifurcation diagram, i.e. for new peaks in self-pulsations, is

$$\frac{dx}{dt} = \frac{d^2x}{dt^2} = 0. \quad (6)$$

According to Eq. (1), this implies having

$$\frac{d^2x}{dt^2} = k \left[ \frac{dx}{dt} f(y, z) + x \frac{df(y, z)}{dt} \right] = 0, \quad (7)$$

where  $f(y, z)$  is given by Eq. (5). That this relation is indeed true can be verified numerically without difficulty. As it is obvious, the explicit conditions in Eq. (6) may be used to locate discontinuities in laser self-pulsations.

Summarizing, from the peak-adding cascade in Fig. 2 one realizes the reason behind the emergence of extra peaks in the laser intensity or, equivalently, extra branches in the bifurcation diagrams: they arise from pulse deformations undergone by the oscillations as the parameter varies.

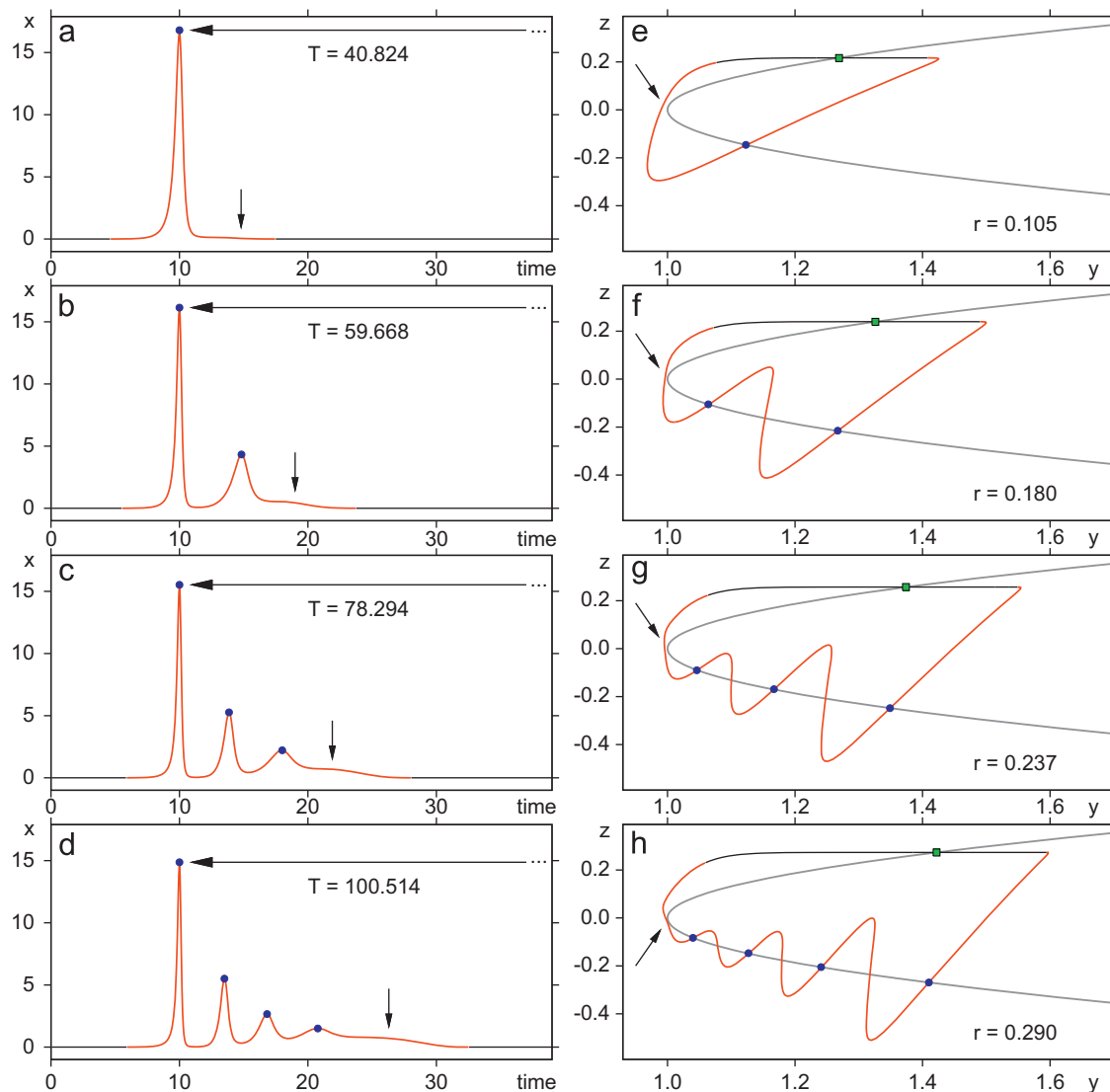


**Fig. 2.** (a)–(d) Laser self-pulsing showing the increase in the number of peaks and in the period as  $r$  increases from  $r=0.105$  (top) to  $r=0.290$  (bottom), as indicated by the four white points along the black line in Fig. 1. Vertical arrows mark the “precursor” of a new spike. (e)–(h) Intersections of  $(y,z)$  trace with  $f(y,z)=0$  (see text). Black segments indicate laser off ( $x < 0.005$ ). The arrows indicate where the next peaks will be born (left column) and the location of the intersections originating them (right column). The green boxes mark the intersections of the laser-off segment of the trajectory with the curve  $f(y,z)=0$ . It has no influence in  $dx/dt$  [see Eq. (1)]. Intersections seen between the blue dots mark local minima of the laser intensity. Note the fast increase of the self-pulsation period  $T$ . Time is measured in  $\mu\text{s}$ . (For interpretation of the references to color in this figure caption, the reader is referred to the web version of this article.)

The isolated extra branches arising through the pulse deformations described here should not be confused with similar discontinuous branches seen in bifurcation diagrams which, however, are due to multistability. The latter involve crossing between *distinct basins of attraction* while in the former the self-pulsation evolves continuously staying always inside *the same basin of attraction*.

### 5. Period discontinuities in self-pulsations

The previous section described peak-adding cascades where the number of laser spikes increased arithmetically and discontinuously when parameters were tuned “diagonally”, i.e. along the general direction represented by the black line in Fig. 1(a). The purpose of this section is to show that discontinuities appear not only in the number of peaks (Fig. 1(a)), but that they also appear in the period (frequency) of the pulses and that they can be of two kinds.

Fig. 3(a) presents a phase diagram showing how the period  $T$  varies as a function of the feedback gain  $r$  and bias voltage  $B$ . In this figure one easily recognizes two dark-green regions, one horizontal, in the upper part of the diagram, and another one roughly parallel to the black line of Eq. (4). Two distinct kinds of discontinuities are observed when varying parameters along the pair of lines depicted in the figure.

The first type of discontinuity is shown in Fig. 3(b) which illustrates how the period evolves along the black line. The inset of this figure shows that a period discontinuity happens inside a very narrow interval, between  $r=0.1416$  and  $r=0.1426$ . These values are plotted as red dots on the black line in Fig. 3(a) which, however, in the scale of the figure, are too close to each other to be distinguished as two distinct points. Between these dots runs a curved vertical discontinuity boundary in the color coding, indicating a discontinuity in  $T$ . This boundary is characterized by jumps similar to the one shown in Fig. 3(b). As this figure shows, additional discontinuities exist which, however, are much less pronounced and whose amplitudes decrease very rapidly.

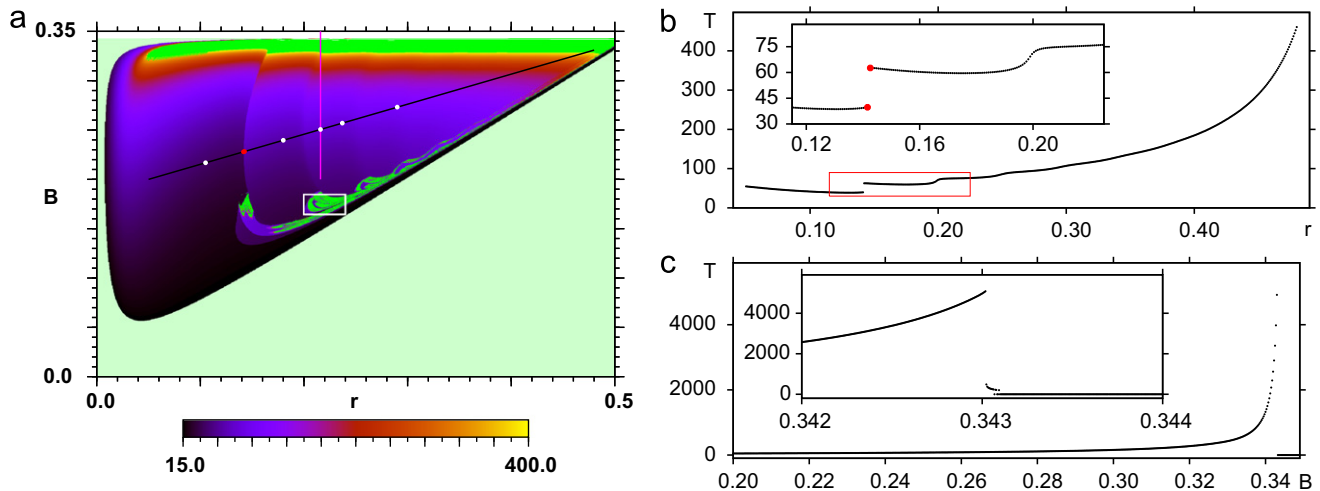


**Fig. 3.** (a) Stability diagram illustrating how the period  $T$  of  $x(t)$  varies as a function of  $r$  and  $B$ . There are several boundaries of discontinuous changes in  $T$ . Along the black line, the largest one is indicated by two (indistinguishable) red dots. The two dark-green regions mark lack of periodicity. (b) Variation of  $T$  along the black line, showing a sharp jump of  $T$  near 0.14 and a smoother one near 0.20. Many other jumps exist, also when varying  $B$ , as indicated by the vertical boundary bracketed by the red dots in (a). (c) Variation of  $T$  along the vertical red line at  $r=0.21593$  showing the divergence responsible for the dark-green horizontal stripe in the upper part of (a).  $B$  and  $r$  are in the same units of Refs. [4–6]. Note that after the divergence of the period there is a narrow region of finite-period near  $B=0.343$ . Multistability is also present in this region. (For interpretation of the references to color in this figure caption, the reader is referred to the web version of this article.)

A second type of discontinuity is shown in Fig. 3(c) and occurs along vertical lines, here  $r=0.21593$ . This particular line was studied by Yang et al. [6] who noted a *divergence* of  $T$  as  $B$  grows. Although the period can be calculated up to very high values, in Fig. 3(a) we introduced a cut-off at  $T=400$ , considering all higher periods as divergences, i.e. as lack of periodicity. This was done to magnify the visibility of the horizontal domain on the top of the figure. Actual divergences occur near the upper boundary of this domain. We stress, however, that the pair of dark-green regions in Fig. 3(a) represents aperiodic pulses of a rather distinct nature. While the horizontal dark-green stripe on the top of the figure marks *divergence of the pulse period*, the other region with a more complex shape, roughly parallel to the black line, marks *non-periodic oscillations*, i.e. chaotic laser pulses.

Comparing Fig. 3(b) and (c) one sees that the nature of the discontinuities along the black line display is much more complex than along the vertical line. Furthermore, comparison of Fig. 1(a) and (a) shows that discontinuities in the number of peaks do not coincide necessarily with discontinuities of the period, a fact clearly borne out in the two-peaks window in the bifurcation diagram in Fig. 1(c).

Using the same representation as in Fig. 2, Fig. 4 shows the cause of the discontinuous period jumps in Fig. 3(b) when passing between  $r=0.1416$  and  $r=0.1426$ . Despite the fact that the red part of the trajectory (representing intervals where  $x > 0$ ) in Fig. 4(c) to be larger than in (d), they both correspond to an essentially identical lapse of time, as can be seen comparing the red segments in Fig. 4(a) and (b). From these figures one may also recognize that in Fig. 4(a) the laser stays considerably longer with  $x=0$  than in Fig. 4(b), what results in a sharp increase of the period. On the other hand, by comparing the black segments in Fig. 4(c) and (d) we see an increase in the inversion  $y$  of the laser such that, when it decays, there is also an increase in the observed laser amplitude.

Finally, Fig. 5 shows details of the laser stability diagram for a parameter region dominated by chaotic self-pulsations. Fig. 5(a) displays  $1200 \times 1200$  Lyapunov exponents used to discriminate chaos (i.e. positive exponents, shown in colors) from periodic pulses (negative exponents). The Lyapunov exponent distribution agrees well with the phase diagram based on the number of peaks in Fig. 5(b) where colors emphasize periodic

pulsations. This figure contains three line segments for which we computed bifurcation diagrams, given in the left column. In the bifurcation diagram of Fig. 5(c) there is a discontinuity in the number of peaks along the leftmost line in Fig. 5(b), similar to the ones described above. However, the sequence of bifurcations along the two remaining line segments display peak-adding cascades of the more common type, namely, cascades mediated by windows of chaotic pulses, observed previously in other systems [29,30]. Note that the pair of peak-adding cascades converge toward a wide accumulation horizon [28] characterized by three-peak pulses, the same number of pulses by which the cascades increase from shrimp to shrimp. This regular organization was observed before for an optically injected semiconductor laser [28]. Thus, while in some regions of the control parameter space one observes novel discontinuous phenomena associated with pulse deformations, it is also possible to find wide parameter regions where the organization is of the more frequently reported kind. The abrupt disruption of cascades of stability regions by the appearance of new peaks arising from pulse deformations shows that, while stability phases may display identical shapes in control parameter space, their inner distribution of pulses may be rather distinct.

## 6. Conclusion and outlook

In conclusion, we described in detail several characteristics of self-pulsations obtained from a systematic numerical investigation of a CO<sub>2</sub> laser with feedback. Self-pulsations were shown to display continuous deformations of their waveforms as parameters are varied. Such deformations create and destroy peaks in the oscillatory patterns. Peak creation and destruction results in rich and intricate *isolated* branches appearing and disappearing in bifurcation cascades. As a result of the added flexibility of incorporating an odd number of branches, sequences of branching cascades for the laser may emerge in rich combinations of the familiar adding and doubling bifurcations something that, we believe, was not yet appreciated. Such branching cascades in the number of peaks of the self-pulsations produce highly intricate mosaics of periodicity domains in control parameter space as exemplified in Figs. 1(b) and 5.

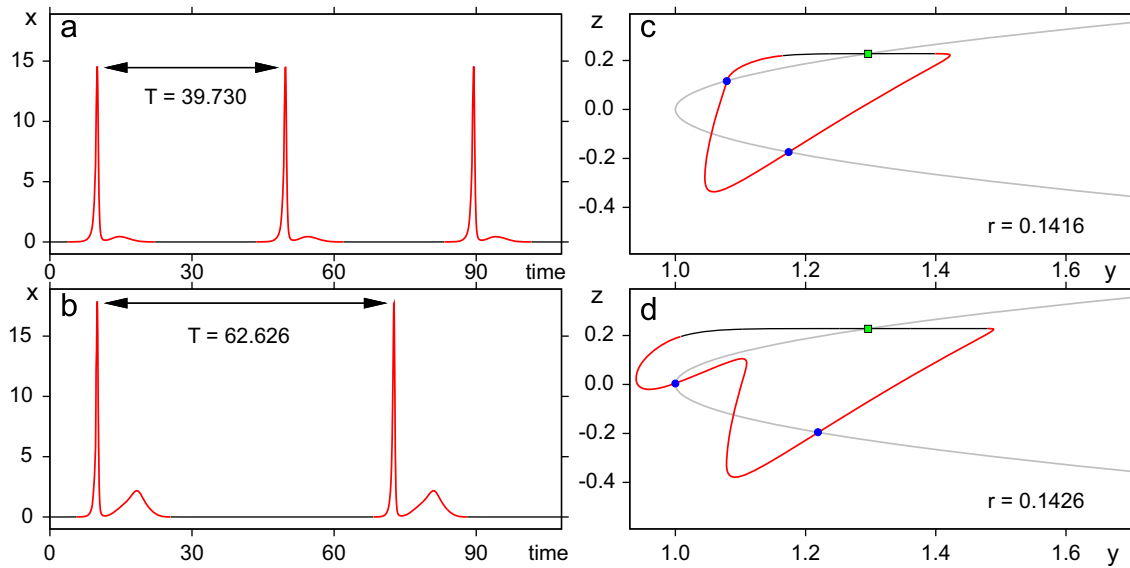


**Fig. 4.** Large jump in the self-pulsing period  $T$  and in the laser intensity observed when changing  $r$  very mildly, from  $r=0.1416$  to  $r=0.1426$ . These jumps are the same ones described in Figs. 1 and 3. In both cases, before and after the jump, the laser pulse has two peaks per period. Black segments indicate that the laser is off ( $x < 0.005$ ). Green boxes mark the intersection of the laser-off segment of the trajectory with the curve  $f(y,z) = 0$ . Time is measured in  $\mu\text{s}$ . (For interpretation of the references to color in this figure caption, the reader is referred to the web version of this article.)

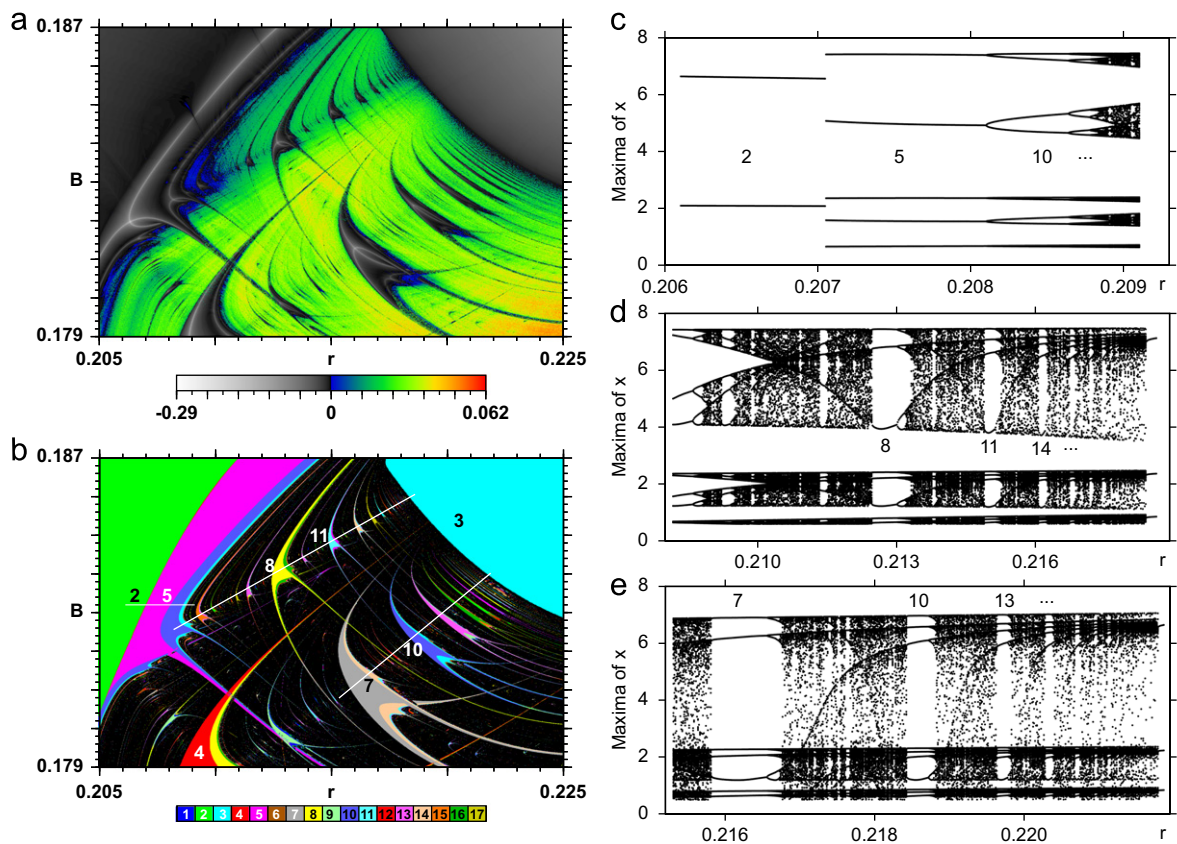


**Fig. 5.** Regular organization of stable self-pulsations in control space. (a) Phase diagram of Lyapunov exponents, with colors emphasizing the extension of the chaotic phase. (b) Phase diagram based on the number of peaks of the laser intensity, with colors emphasizing periodicity islands. Along the pair of non-horizontal lines one finds peak-adding shrimp cascades mediated by chaos. Numbers refer to the number of spikes in the laser intensity. (c)–(e) Bifurcations diagrams along the three lines shown in (b). Note that the pair of chaos-mediated peak-adding shrimp cascades occur along very particular “directions” [23] and converge towards a large three-spikes accumulation horizon [28]. In (b) colors are recycled modulo 17. See text.  $B$  and  $r$  are in the same units of Refs. [4–6]. (For interpretation of the references to color in this figure caption, the reader is referred to the web version of this article.)

Note that the sequence of small pulses following the fundamental one in figures such as Fig. 2(b)–(d) decay with a decreasing rate as the coupling  $r$  is increased, but the separation between

the pulses has roughly the same duration. A simple calculation of the solitary laser equations with zero feedback shows that the period of the relaxation frequency is of the order of  $6 \mu\text{s}$  and,

indeed, corresponds to the period of the decaying relaxation oscillations that follow the main peak. Additionally, as  $r$  is increased, it affects the damping of the laser, which decreases. Therefore, the pulsations following the main one are sustained longer. In this context, an interesting problem is to compute some of the spectra of the time series to characterize the fundamental frequency structures with and without feedback.

We hope that peak-adding cascades not mediated by chaos as well as the discontinuities in the frequency and laser intensity reported here may motivate their experimental corroboration in the near future. A few simple ways of recording experimentally novel phenomena in laser stability diagrams were discussed recently for a semiconductor laser with optoelectronic feedback [31] (see also Ref. [32]). An interesting related problem is to extend our stability diagrams by investigating systematically the distribution of self-pulsing when a *delayed* feedback is added [14–19]. Results for the CO<sub>2</sub> laser and for some laser diodes showing a number of remarkable features are being finalized for publication [20].

### Acknowledgments

The authors thank Prof. Thorsten Pöschel for the invitation and kind hospitality at the Friedrich-Alexander Universität Erlangen-Nürnberg. This work was supported by the Deutsche Forschungsgemeinschaft through the Cluster of Excellence *Engineering of Advanced Materials*. LJ is supported by a CNPq Doctoral Fellowship. JACG is supported by CNPq and AFOSR, grant FA9550-07-1-0102. All bitmaps were computed in the CESUP-UFRGS clusters.

### References

- [1] R.W. Fox, C.W. Oates, L. Hollberg, Stabilizing diode lasers to high finesse cavities, in: *Experimental Methods in the Physical Sciences*, vol. 40, Elsevier, Amsterdam, 2001 (Chapter 1).
- [2] J. Ohtsubo, *Semiconductor Lasers: Stability, Instability and Chaos*, Springer, New York, 2005.
- [3] D.M. Kane, K.A. Shore, *Unlocking Dynamical Diversity: Optical Feedback Effects on Semiconductor Lasers*, Wiley, New York, 2005.
- [4] F.T. Arecchi, W. Gadamski, R. Meucci, *Physical Review A* 34 (1986) 1617.
- [5] P.Y. Wang, A. Lapucci, R. Meucci, F.T. Arecchi, *Optics Communications* 80 (1990) 42.
- [6] Q.S. Yang, P.Y. Wang, H.W. Yin, J.H. Dai, H.J. Zhang, *Optics Communications* 138 (1997) 325.
- [7] W. Vandermeiren, J. Stiens, G. Shkerdin, R. Vounckx, *IEEE Journal of Quantum Electronics* 48 (2012) 447.
- [8] J.P. Toomey, C. Nichkawde, D.M. Kane, K. Schires, I.D. Henning, A. Hurtado, M.J. Adams, *Optics Express* 20 (2012) 10256.
- [9] M.-N. Tang, *Chinese Physics B* 21 (2012) 020509.
- [10] L. Illing, G. Hoth, L. Shareshian, C. May, *Physical Review E* 83 (2011) 026107.
- [11] Y. Cho, T. Umeda, *Optics Communications* 59 (1986) 131.
- [12] F.T. Arecchi, G. Giacomelli, A. Lapucci, R. Meucci, *Physical Review A* 43 (1991) 4997.
- [13] J.L. Chern, K. Otsuka, F. Ishiyama, *Optics Communications* 96 (1993) 259.
- [14] Y.C. Koumou, P. Colet, L. Larger, N. Gastaud, *IEEE Journal of Quantum Electronics* 41 (2005) 156.
- [15] J. Scheuer, A. Yariv, *Physical Review Letters* 97 (2006) 140502.
- [16] D.S. Yee, Y.A. Leem, S.T. Kim, K.H. Park, B.G. Kim, *IEEE Journal of Quantum Electronics* 43 (2007) 1095.
- [17] R.M. Nguimdo, P. Colet, L. Larger, L. Pesquera, *Physical Review Letters* 107 (2011) 034103.
- [18] E.J. Bochove, A.B. Aceves, Y. Braiman, P. Colet, R. Deiterding, A. Jacobo, C.A. Miller, C. Rhodes, S.A. Shakir, *IEEE Journal of Quantum Electronics* 47 (2011) 777.
- [19] R.E. Francke, T. Pöschel, J.A.C. Gallas, Infinite networks of hubs, spirals, and zig-zag patterns in self-sustained oscillations of a tunnel diode and of an erbium-doped fiber-ring laser, Springer, Berlin, in press.
- [20] L. Junges, J.A.C. Gallas, Manuscript, in preparation.
- [21] J.G. Freire, J.A.C. Gallas, *Physical Chemistry Chemical Physics* 13 (2011) 12191; J.G. Freire, J.A.C. Gallas, *Physics Letters A* 375 (2011) 1097.
- [22] L. Junges, J.A.C. Gallas, *Physics Letters A* 376 (2012) 2109.
- [23] J.A.C. Gallas, *Physical Review Letters* 70 (1993) 2714.
- [24] J.A.C. Gallas, *Applied Physics B* 60 (1995) S203; J.A.C. Gallas, *Physica A* 202 (1994) 196; J.A.C. Gallas, *International Journal of Bifurcation and Chaos* 20 (2010) 197.
- [25] E.N. Lorenz, *Physica D* 237 (2008) 1689.
- [26] R. Vitolo, P. Glendinning, J.A.C. Gallas, *Physical Review E* 84 (2011) 016216.
- [27] D.F.M. Oliveira, E.D. Leonel, *Chaos* 21 (2011) 043122; D.F.M. Oliveira, E.D. Leonel, *New Journal of Physics* 13 (2011) 123012.
- [28] C. Bonatto, J.A.C. Gallas, *Physical Review E* 75 (2007) 055204(R); C. Bonatto, J.A.C. Gallas, *Philosophical Transactions of the Royal Society of London* 366A (2008) 505.
- [29] C. Bonatto, J.C. Garreau, J.A.C. Gallas, *Physical Review Letters* 95 (2005) 143905.
- [30] C. Bonatto, J.A.C. Gallas, *Physical Review Letters* 101 (2008) 054101.
- [31] J.G. Freire, J.A.C. Gallas, *Physical Review E* 82 (2010) 037202.
- [32] V. Kovanis, A. Gavrielides, J.A.C. Gallas, *European Physical Journal D* 58 (2010) 181.